symmetry

MDPI

Article

Transverse Force Analysis of Adjacent Shield Tunnel Caused by Foundation Pit Excavation Considering Deformation of Retaining Structures

Xinhai Zhang [1,2], Gang Wei [1,*], Xinbei Lin [3], Chang Xia [4] and Xinjiang Wei [1]

[1] Department of Civil Engineering, Zhejiang University City College, Hangzhou 310015, China; zhangxinhai@zju.edu.cn (X.Z.); weixj@zucc.edu.cn (X.W.)
[2] Ocean College, Zhejiang University, Zhoushan 316021, China
[3] College of Civil Engineering, Zhejiang University of Technology, Hangzhou 310023, China; 2112006146@zjut.edu.cn
[4] Fuzhou Planning & Design Research Institute Group Co., Ltd., Fuzhou 350108, China; xiac@fzghy.com
* Correspondence: weig@zucc.edu.cn; Tel.: +86-5718-801-2136

Abstract: In order to research the theory for the variety of transverse forces of the adjacent shield tunnels caused by foundation pits excavation, the effect mechanism of foundation pit excavation on the adjacent shield tunnel was analyzed. The sidewall unloading model of the foundation pit, considering the deformation of the retaining structures, was introduced to calculate the additional stress of soil caused by foundation pit excavation. On this basis, the additional confining pressure variation model of the adjacent shield tunnel was established, considering the influence of the longitudinal deformation. Take the deep foundation pit project by the side of the shield tunnel of Hangzhou Metro Line 2 as a case study, the variation in confining pressure distribution of the adjacent shield tunnel caused by foundation pit excavation was analyzed, and a simplified finite element model was established to calculate the internal force of the segment ring structure. Moreover, the influence factors were analyzed, such as the deformation of the foundation pit retaining structure, the clearance between the foundation pit and the adjacent tunnel, and the buried depth of the tunnel. The present study suggests that the foundation pit excavation reduces the confining pressure of the adjacent shield tunnel, increases the absolute value of bending moment and shear force, and decreases the axial force at the top and bottom of the tunnel's segment ring. With the increase in the deformation of the foundation pit's retaining structure, the absolute value of the additional confining pressure on the adjacent tunnel increases, and the response of the bending moment to the foundation pit excavation unloading is more obvious than the variation in the confining pressure. When the buried depth of the adjacent shield tunnel is deeper than the excavation depth of the foundation pit, the influence of the excavation on the tunnel will be obviously weakened. With the decrease in the distance between the pit and tunnel, the influence of the excavation on the tunnel will be enhanced.

Keywords: sidewall unloading of foundation pit; deformation of the retaining structures; adjacent shield tunnel; additional confining pressure; transverse force

check for updates

Citation: Zhang, X.; Wei, G.; Lin, X.; Xia, C.; Wei, X. Transverse Force Analysis of Adjacent Shield Tunnel Caused by Foundation Pit Excavation Considering Deformation of Retaining Structures. *Symmetry* **2021**, *13*, 1478. https://doi.org/10.3390/sym13081478

Academic Editor: Raffaele Barretta

Received: 1 July 2021
Accepted: 9 August 2021
Published: 12 August 2021

Publisher's Note: MDPI stays neutral with regard to jurisdictional claims in published maps and institutional affiliations.

Copyright: © 2021 by the authors. Licensee MDPI, Basel, Switzerland. This article is an open access article distributed under the terms and conditions of the Creative Commons Attribution (CC BY) license (https://creativecommons.org/licenses/by/4.0/).

1. Introduction

With the development and utilization of underground space, many cases of foundation pit construction at the side of the existing shield tunnel have appeared in many cities. For example, the foundation pit of Jing'an Jiali block located in the south of Shanghai Metro Line 2 is only 8 m away from the shield tunnel [1]. The closest distance between the foundation pit of a building on the north side of Suzhou Metro Line 4 and the metro tunnel is about 9 m [2]. The sidewall unloading effect of foundation pit excavation will cause an additional load to the adjacent tunnel, which will harm the existing shield tunnel structure. For instance, the foundation pit of the Ningbo C1-6/7 block caused a large deformation of

the shield tunnel nearby, resulting in segment structure cracking and damage [3]. All these will have a great impact on the safety of shield tunnel operation, so it is necessary to study the force and deformation of the shield tunnel by the side of the foundation pit.

This kind of engineering problem has aroused attention at home and abroad. At present, the main research methods include theoretical calculation [4–9], numerical simulation [10–13], centrifuge test [14], and measured data analysis [15,16]. In the calculation methods studied for this problem, there are two categories that can be classified broadly. The first one treats the structures and their surrounding soil as a whole analysis, and this is often conducted using commercial software. Among them, the three-dimensional finite element method can consider the complex boundary conditions and the interaction between structures and their surrounding soil. Therefore, it is widely used in the study of the influence of foundation pit excavation on adjacent tunnels [12,13]. However, it requires professional software and substantial computational effort, and it is only suitable for obtaining some details in a final design rather than as a preliminary routine design tool. The other category, the so-called two-stage method, can divide the complex interactional problem into two simple stages. The first stage is calculating the stress or free soil deformation at the locations of existing structures. In the second stage, the stress or free soil deformation is then imposed on the existing structures in the analyses of computing the responses of the structures by using mechanical calculation models. The two-stage method is a suitable choice to analyze the behavior of existing structures affected by nearby construction, especially for the preliminary design and construction adjustment. Therefore, this method has also been used to perform some analysis on the response of adjacent tunnels due to foundation pit excavation [6–9].

Currently, these existing theoretical calculation studies pay more attention to the longitudinal deformation of the shield tunnel, and the research results of the shield tunnels' confining pressure changes caused by the foundation pit excavation are mainly obtained by numerical simulation [17] and laboratory experiments [18]. There are few studies on theoretical calculation methods. Wei et al. [19] have proposed the theoretical calculation method for the variety in the confining pressure of the shield tunnel caused by foundation pit excavation, but it cannot consider the deformation of the retaining structure of the foundation pit. Furthermore, the unloading model of the foundation pit is far from the actual situation, and the influence of the force between the segment rings of the tunnel on the transverse force is also insufficiently considered. Authors [20] have considered the deformation of the foundation pit' retaining structures and the partition of the region affected in the study of the influence of the foundation pit on the adjacent shield tunnel, which compensates for the deficiencies of the existing foundation pit unloading model. However, it focuses on the longitudinal deformation of shield tunnels, without considering the variety in the tunnel's confining pressure and structural's transverse force. Therefore, it is necessary to deeply study the theory for the variety in the confining pressure and transverse forces of the shield tunnels by the adjacent foundation pits.

In this paper, the effect mechanism of the unloading of the foundation pit's sidewall on the adjacent shield tunnel is analyzed. An unloading model of the sidewall is introduced, which both considers the deformation of the foundation pit's retaining structure and the spatial effect. An additional confining pressure change model for the shield tunnel is established, considering the effect of longitudinal deformation. In accordance with engineering examples, the variation in confining pressure distribution of the shield tunnel beside the foundation pit is analyzed, and a simplified finite element model is established to calculate the internal force changes of the segment ring structure. Moreover, the influencing factors are analyzed, such as the deformation control value of the foundation pit's retaining structure, the clearance between the foundation pit's retaining structure and the adjacent tunnel, and the depth of the adjacent shield tunnel.

2. Research on Sidewall Unloading of Foundation Pit

2.1. The Deficiency of the Existing Foundation Pit Unloading Model

When studying the influence of the foundation pit excavation on the nearby shield tunnel, the distribution of soil additional stress caused by unloading should be calculated first. The choice of foundation pit unloading model will directly affect the calculation results of soil additional stress distribution. Zhou et al. [21] believed that stress release on the sidewall was all balanced by the support system, and the sidewall of the foundation pit had no unloading effect on the soil, as shown in Figure 1a. In engineering practice, all the foundation pits retaining structures will deform inevitably, and the sidewalls will have the corresponding unloading effect on the soil. Especially for the shield tunnel by the side of the foundation pit, the unloading effect of the adjacent sidewalls cannot be ignored. Zhang et al. [5] took the static earth pressure with triangular distribution as sidewall unloading, and the unloading effects of all sidewalls of foundation pit is superimposed during the calculation process, as shown in Figure 1b, but did not divide the area affected by the sidewall. Jiang et al. [22] believed that only the unloading effect of the foundation pit's sidewall adjacent to the tunnel should be taken into account, and the static earth pressure at the retaining structure was also used as the unloading, as shown in Figure 1c. This method theory does not consider the role of the retaining structure in bearing earth pressure, which was not reasonable for the internal support structure with enough stiffness.

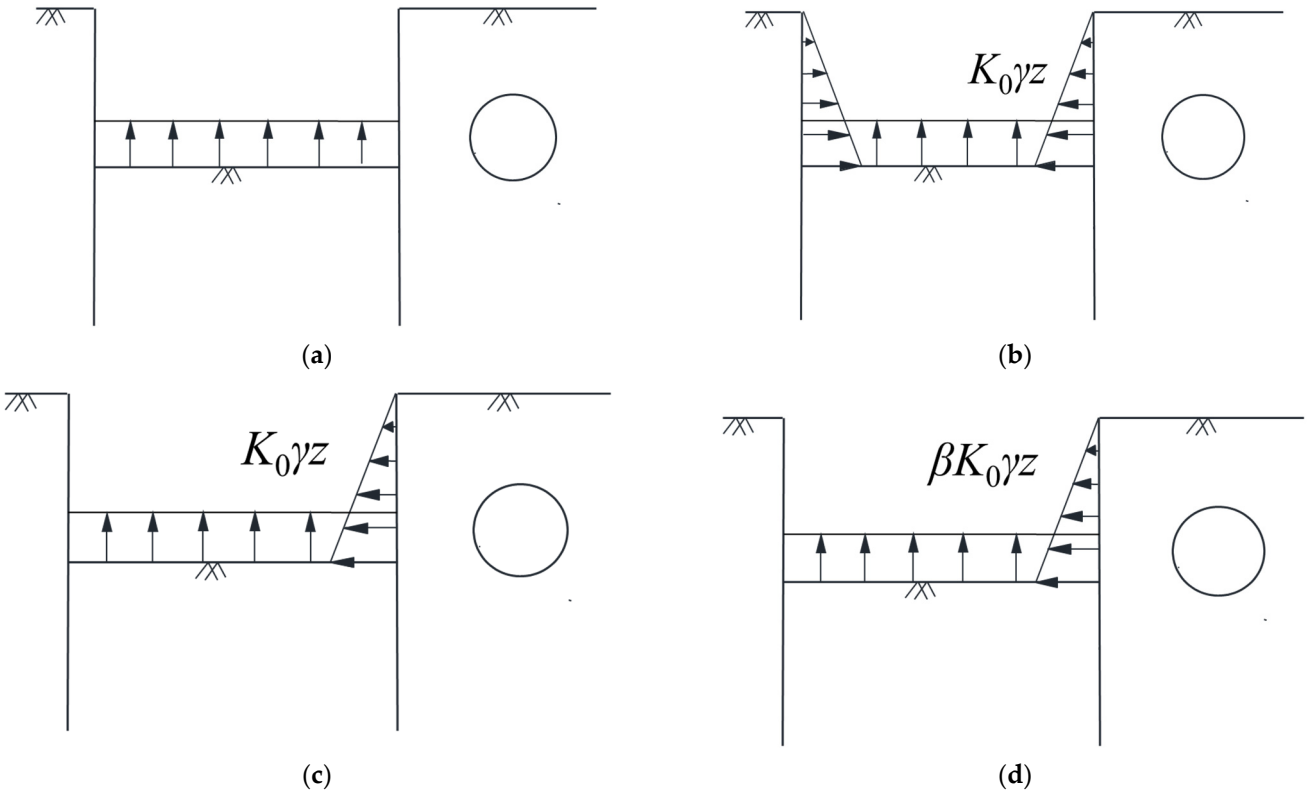


Figure 1. Schematic diagram of foundation pit unloading model. (**a**) Unloading model I (Zhou et al. [21]), (**b**) Unloading model II (Zhang et al. [5]), (**c**) Unloading model III (Jiang et al. [22]), (**d**) Unloading model IV (Wei et al. [23]).

For such deficiencies, Wei et al. [23] introduced the stress loss rate β of the foundation pit retaining structure in the study to consider the partial release of the stress on the sidewall of the foundation pit under the action of the retaining structure, as shown in Figure 1d. The results show that the value of stress loss rate β greatly influences the calculation results. Moreover, this method simplifies the distribution of unloading greatly and cannot consider the deformation of the retaining structure and the spatial effect of the foundation pit.

In the application of practical engineering, the earth pressure on the retaining structure will gradually decrease during the foundation pit excavation because of the deformation of the retaining structure. It is hard to obtain the value of stress release rate (the ratio of the earth pressure decrease in the retaining structure to the static earth pressure), and it is also difficult to introduce this parameter as a control index in the design stage of the foundation pit, and therefore, it is not available to apply it to the protection design of the shield tunnel beside foundation pit at present. Therefore, it is necessary to put forward a more reasonable sidewall unloading model of foundation pit, which can consider the influence of deformation of retaining structures and spatial effect of foundation pit and also serve as a reference for the design of foundation pit adjacent to the tunnel.

2.2. A Sidewall Unloading Model Considering the Deformation of Retaining Structure

The design theory of controlling deformation has been widely used in foundation pit engineering. It is crucial to control the effect of the foundation pit excavation on the adjacent shield tunnel by taking the deformation of the retaining structure as the control index in the design stage. Therefore, it is more reasonable to adopt the sidewall unloading model considering the deformation of the retaining structure when studying the influence of the foundation pit excavation on the nearby shield tunnel.

Figure 2 is the deformation diagram for the sidewall retaining structure of the foundation pit. As shown in the figure, the retaining structure deforms under the action of soil pressure in the process of excavation, where H is the height of the retaining structure within the influence scope of deformation. When the toe of the retaining structure is inserted into the stiff soil layer, H is the distance between the retaining structure's coping and the stiff soil layer below the excavation face. H_e is the excavation depth. λ is the horizontal distance between any point on the retaining structure and the foundation pit corner. η is the buried depth at any point on the sidewall of the retaining structure. Set the displacement of any point on the retaining structure of the sidewall toward the inside of the foundation pit as $v(\lambda, \eta)$.

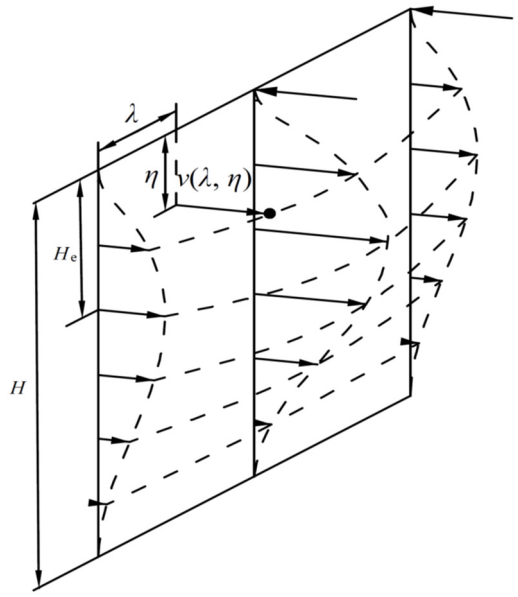


Figure 2. Deformation diagram of sidewall retaining structure.

According to the research of Ding et al. [24], the displacement curve of deep foundation pit sidewall in the soft soil area of Zhejiang Province is mainly dominated by the arch, especially when the top of the flexible retaining structure installed the inner support with enough stiffness, the retaining structure presents a deformation behavior with small displacement at both ends and protruding toward the inside of foundation pit in the middle.

Liu et al. [25] fitted the deformation increment of retaining structure with piecewise cosine function. According to the current engineering statistics, it was found that the buried depth of the maximum deformation increment of the foundation pit with the inner support was located near the excavation face. Hence, the deformation increment of the retaining structure sidewall can be expressed as

$$\left.\begin{array}{ll} \delta_i(\eta, H_{ei}) = \frac{\delta_{maxi}}{2}\left[1-\cos\left(\frac{\pi\eta}{H_{ei}}\right)\right] & (0 \le \eta \le H_{ei}) \\ \delta_i(\eta, H_{ei}) = \frac{\delta_{maxi}}{2}\left\{1-\cos\left\{\frac{\pi[\eta+(H-2H_{ei})]}{H-H_{ei}}\right\}\right\} & (H_{ei} \le \eta \le H) \end{array}\right\} \quad (1)$$

where $\delta_i(\eta, H_{ei})$ is the deformation increment of the sidewall retaining structure at the depth η of the foundation pit caused by the excavation of the i-th layer, while H_{ei} is the depth of the excavation face after the excavation of the i-th layer. $\delta_{max\,i}$ is the maximum deformation increment of the sidewall retaining structure caused by the excavation of the i-th layer. The applications of engineering generally use the accumulated maximum deformation of the retaining structure as the control index. This paper selects the ratio of accumulated maximum deformation of the retaining structure to the excavation depth as the control parameter of the retaining structure's deformation during design and calculation. The accumulated deformation satisfies the control values when excavated each soil layer; therefore, the maximum deformation increment of the i-th layer excavation can be represented as

$$\left.\begin{array}{ll} \delta_{maxi} = \frac{v_{max}}{H_e} \cdot H_{ei} & (i = 1) \\ \delta_{maxi} = \frac{v_{max}}{H_e} \cdot H_{ei} - \sum_{j=1}^{i-1} \delta_j(H_{ei}) & (i \ge 2) \end{array}\right\} \quad (2)$$

where v_{max} is the accumulated maximum deformation of the retaining structure caused by the excavation of the foundation pit; H_e is the excavation depth of the foundation pit; δ_j (H_{ei}, H_{ej}) is the deformation increment of the sidewall retaining structure at the depth H_{ei}, caused by the excavation of the j-th layer in the foundation pit; H_{ej} is the depth of the excavation face after the excavation of the j-th layer.

In the foundation pit design, the problem of the foundation pit is often simplified as a plane strain problem. However, in practical engineering, the deformation of the foundation pit presents an obvious spatial effect. As shown in Figure 3, due to the different stiffness of the support structure system and stress state of the soil, the deformation of the area close to the corner of the foundation pit is small, while the deformation of the central area of the longer retaining structure is large, which is approximate to the deformation under the plane strain condition. OU et al. [26] introduced the ratio of plane strain (PRS) to quantitatively describe the influence of spatial effect, which is the ratio of displacements of soil mass or retaining structure under three-dimensional simulation to the displacements under plane strain. Liu et al. [27] studied the spatial effect of inner bracing foundation pit with different retaining structures. The results showed that the PSR variation trend of the underground diaphragm wall retaining structure was similar to the fitting formula curve proposed by Finno et al. [28] When the PSR is close to 1.00, the value of corresponding λ/H_e is 4.00, and the PSR near the corner was 0.72. By substituting into the fitting formula, the following equation can be obtained:

$$\left.\begin{array}{ll} PSR(\lambda, H_e) = 1.671 - e^{-0.1\lambda/H_e} & (0 \le \lambda < 4H_e) \\ PSR(\lambda, H_e) = 1 & (\lambda \ge 4H_e) \end{array}\right\} \quad (3)$$

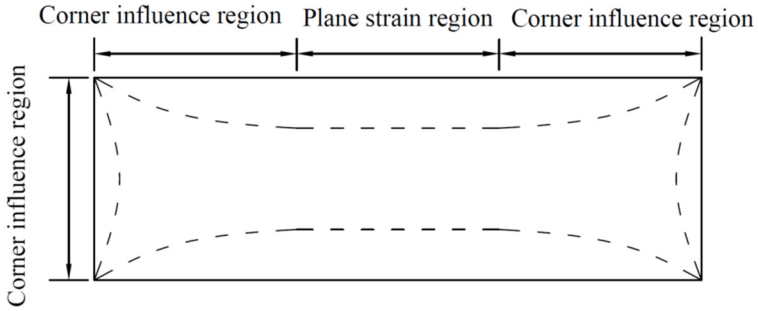


Figure 3. Schematic diagram for the spatial effect of foundation pit.

By integrating Equations (1)–(3), the calculation formula of the retaining structure's deformation increment at any position of the sidewall during the excavation of each layer after considering the spatial effect can be obtained as follows:

$$\delta_i'(\lambda, \eta, H_{ei}) = \mathrm{PSR}(\lambda, H_{ei}) \cdot \delta_i(\eta, H_{ei}) \tag{4}$$

When n-th layers are excavated in the foundation pit and the depth of the excavation face reaches H_e, the cumulative deformation distribution of the retaining structure is as follows:

$$v(\lambda, \eta) = \sum_{i=1}^{n} \delta_i'(\lambda, \eta, H_{ei}) \tag{5}$$

where the excavation depth of the foundation pit is the sum of the thickness of each layer excavated before $H_e = H_{e1} + \sum_{i=2}^{n} \left(H_{ei} - H_{e(i-1)} \right)$.

In terms of the theoretical calculation of earth pressure, some researchers in China have given a variety of approximate calculation methods for active earth pressure considering displacement, among which, the expression of tangent function to simulate the relationship between relaxation stress and displacement proposed by Xu [29] is relatively simple, which is suitable to the simplified calculation of soil pressure on retaining structure. Based on this theory, the calculation formula of soil pressure at any point outside the retaining structure can be obtained as follows:

$$e_a(\lambda, \eta) = e_0(\lambda, \eta) + \sin\left(\frac{\pi}{2} \cdot \frac{v(\lambda, \eta)}{v_{acr}} \right) [e_{acr}(\lambda, \eta) - e_0(\lambda, \eta)] \tag{6}$$

where $e_0(\lambda, \eta)$ and $e_{acr}(\lambda, \eta)$ are the static earth pressure and active earth pressure under the limit state, respectively, obtained from the distribution of the soil layer outside the foundation pit, and v_{acr} is the displacement required when the soil is in the active limit state, generally taking v_{acr} = 0.001~0.003 H [30].

The unloading of the foundation pit sidewall can be considered as the difference between the static earth pressure at the initial state and the retaining structure's lateral load after excavation. Therefore, the unloading of the sidewall can be expressed as

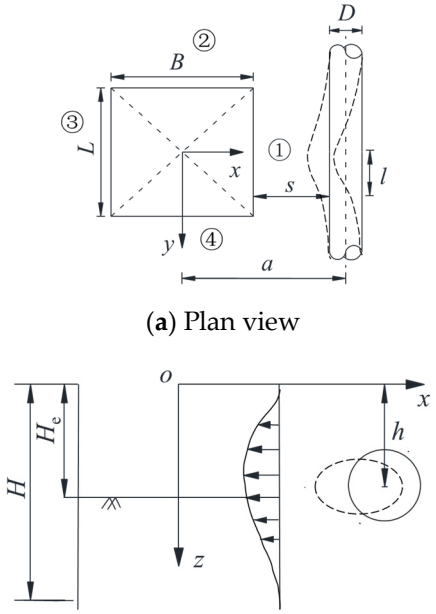
$$p_c(\lambda, \eta) = e_0(\lambda, \eta) - e_a(\lambda, \eta) = \sin\left(\frac{\pi}{2} \cdot \frac{v(\lambda, \eta)}{v_{acr}} \right) [e_0(\lambda, \eta) - e_{acr}(\lambda, \eta)] \tag{7}$$

3. Confining Pressure Change of Shield Tunnel beside Foundation Pit

3.1. Calculation Model and the Area Division of Unloading Impact

The theoretical model for calculating is shown in Figure 4a,b. A coordinate system is established at the center of the foundation pit on the ground as the origin. The rectangular foundation pit is excavated by the side of the shield tunnel. The x-axis and y-axis are perpendicular and parallel to the tunnel axis, respectively, and the positive direction of z-axis is vertically downward. The excavation size along the y-axis is L, the excavation size

along the x-axis is B, and the excavation depth of the foundation pit is H_e. The horizontal distance between the axis of the tunnel and the center of the foundation pit is a, the outer diameter of the shield tunnel is D, the buried depth of the tunnel's axis is h, and the minimum clearance between the retaining structure and the tunnel is s ($s = a\text{-}B/2\text{-}D/2$). The height of the retaining structure within the scope of deformation is H. Therefore, it can be obtained that the coordinate of any point on the tunnel axis is (a, l, h), where l is the horizontal distance between the calculation point on the tunnel along the y-axis and the excavation center of the foundation pit.



(**a**) Plan view

(**b**) Section view

Figure 4. The schematic diagram of the position relationship and influence between the foundation pit and the adjacent shield tunnel.

As shown in Figure 4a, the serial numbers of the four sidewalls are ①, ②, ③, ④, respectively. According to the analysis, the interval between the foundation pit sidewall (③) and the tunnel is an open space in which the soil has been removed; therefore, the unloading effect of sidewall ③ cannot be passed to the tunnel. Thus, this paper only considered the unloading effect of sidewalls ①, ②, ④ when calculating the additional stress on the tunnel. Meanwhile, this paper divides the impact region on the tunnel, which is affected by the unloading of each sidewall. As shown in Figure 5, the whole impact region can be divided into three parts. The central area of the whole impact region is mainly affected by the unloading of sidewall ①. The left side of the whole impact region is affected by the common impact of sidewalls ① and ④. The right side of the whole impact region is affected by the common impact of sidewalls ① and ②.

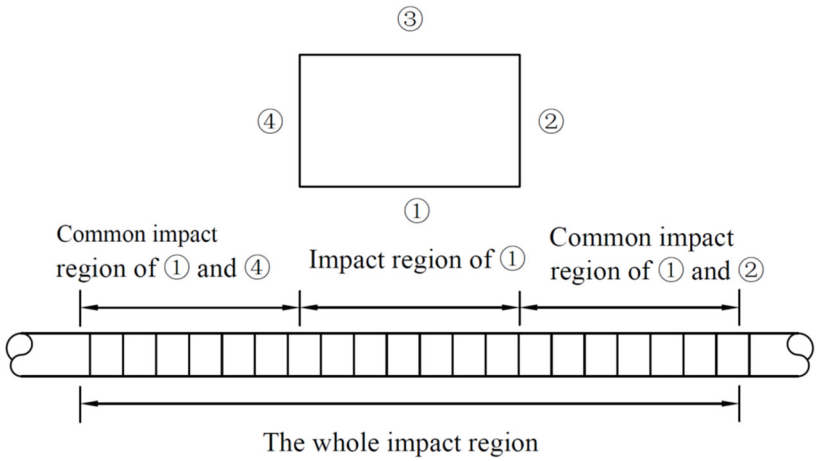


Figure 5. The schematic diagram about the partition of region affected by the unloading of sidewall.

3.2. Additional Stress of the Soil around the Shield Tunnel by the Adjacent Foundation Pit

Referring to the method in the literature [19], taking an infinitesimal element $d\zeta d\eta$ at point $(B/2, \zeta, \eta)$ on sidewall ①, substitute the unloading of the sidewall $p_c(L/2-\zeta, \eta)$ (the specific calculation formula is shown in Equation (7)) and the positional relation into the Mindlin stress solution [31], and integrate to obtain the additional stress of the soil around the side tunnel caused by the unloading of sidewall ① along the x-axis direction and z-axis direction, respectively, for

$$\sigma_{ax1}(\theta, l) = -\int_0^{H_e}\int_{-L/2}^{L/2} p_c(L/2-\zeta,\eta)\cdot\sigma_{xx}(a+\frac{D\sin\theta}{2}, l, h-\frac{D\cos\theta}{2}, B/2, \zeta, \eta)d\zeta d\eta \quad (8)$$

$$\sigma_{az1}(\theta, l) = -\int_0^{H_e}\int_{-L/2}^{L/2} p_c(L/2-\zeta,\eta)\cdot\sigma_{zx}(a+\frac{D\sin\theta}{2}, l, h-\frac{D\cos\theta}{2}, B/2, \zeta, \eta)d\zeta d\eta \quad (9)$$

where σ_{xx} and σ_{zx} are the Mindlin stress solutions [31] in the x-axis and z-axis directions caused by the unit force in the x-axis direction, respectively; θ is the position angle (° or rad) of the calculation point on the tunnel's segment rings, and the upper vertex is 0°, the angle increases in the clockwise; ζ and η are integral variables for the integral operation.

Referring to the method in the literature [19], taking an infinitesimal element $d\xi d\eta$ at point $(\xi, -L/2, \eta)$ on sidewall ②, substitute the unloading of the sidewall $p_c(B/2-\xi, \eta)$ (the specific calculation formula is shown in Equation (7)) and the positional relation into the Mindlin stress solution [31], considering the division of the affected area in Section 3.1, the additional stress of the soil around the side tunnel caused by the unloading of sidewall ② along the x-axis direction and z-axis direction are obtained by integrating, respectively, for

$$\left.\begin{array}{ll}\sigma_{ax2}(\theta, l) = \int_0^{H_e}\int_{-B/2}^{B/2} p_c(B/2-\xi,\eta)\cdot\sigma_{xy}(a+\frac{D\sin\theta}{2}, l, h-\frac{D\cos\theta}{2}, \xi, -L/2, \eta)d\xi d\eta & l\in(-\infty, -L/2] \\ \sigma_{ax2}(\theta, l) = 0 & l\in(-L/2, +\infty)\end{array}\right\} \quad (10)$$

$$\left.\begin{array}{ll}\sigma_{az2}(\theta, l) = \int_0^{H_e}\int_{-B/2}^{B/2} p_c(B/2-\zeta,\eta)\cdot\sigma_{zy}(a+\frac{D\sin\theta}{2}, l, h-\frac{D\cos\theta}{2}, \xi, -L/2, \eta)d\xi d\eta & l\in(-\infty, -L/2] \\ \sigma_{az2}(\theta, l) = 0 & l\in(-L/2, +\infty)\end{array}\right\} \quad (11)$$

where σ_{xy} and σ_{zy} are the Mindlin stress solutions [31] in the x-axis and z-axis directions caused by the unit force in the x-axis direction, respectively; ξ and η are integral variables for the integral operation.

Similarly, the additional stress of the soil around the side tunnel caused by the unloading of sidewall ④ along the x-axis direction and z-axis direction are as follows:

$$\left.\begin{array}{ll}\sigma_{ax4}(\theta, l) = 0 & l\in(-\infty, L/2] \\ \sigma_{ax4}(\theta, l) = -\int_0^{H_e}\int_{-B/2}^{B/2} p_c(B/2-\xi,\eta)\cdot\sigma_{xy}(a+\frac{D\sin\theta}{2}, l, h-\frac{D\cos\theta}{2}, \xi, L/2, \eta)d\xi d\eta & l\in(L/2, +\infty)\end{array}\right\} \quad (12)$$

$$\left.\begin{array}{ll}\sigma_{az4}(\theta,l)=0 & l\in(-\infty,L/2]\\ \sigma_{az4}(\theta,l)=-\int_0^{H_e}\int_{-B/2}^{B/2}p_c(B/2-\xi,\eta)\cdot\sigma_{zy}(a+\frac{D\sin\theta}{2},l,h-\frac{D\cos\theta}{2},\xi,L/2,\eta)\mathrm{d}\xi\mathrm{d}\eta & l\in(L/2,+\infty)\end{array}\right\} \quad (13)$$

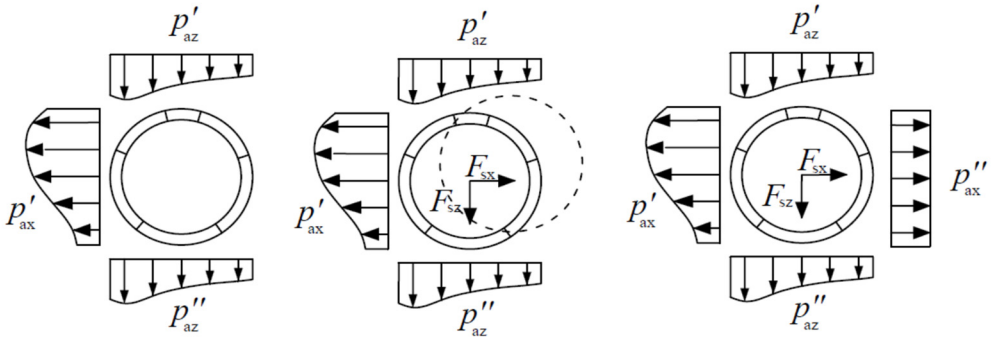
3.3. The Variation in Confining Pressure Considering the Force between the Segment Rings

When the additional loads caused by foundation pit excavation are applied to the tunnel, the longitudinal deformation of the tunnel and the variation in the transverse confining pressure will appear. The confining pressure will redistribute as the cooperative deformation between tunnel and soil. When the tunnel's structure reaches the equilibrium state of force, the confining pressure and deformation are stable. In the actual engineering, the longitudinal deformation of the tunnel and the variation in the transverse confining pressure are carried out at the same time. For the convenience of research, this paper divides this process into three stages to describe.

First of all, as shown in Figure 6a, the excavation of the foundation pit will generate the horizontal additional loads p'_{ax} on the side of the tunnel near the foundation pit and the vertical additional loads p'_{az} and p''_{az} both at the top and bottom of the segment rings. These can be obtained by the following formula:

$$p'_{ax}(\theta,l)=\sigma_{ax1}(\theta,l)+\sigma_{ax2}(\theta,l)+\sigma_{ax4}(\theta,l)\ \pi\le\theta<2\pi \quad (14)$$

$$\left\{\begin{array}{l}p'_{az}(\theta,l)=\sigma_{az1}(\theta,l)+\sigma_{az2}(\theta,l)+\sigma_{az4}(\theta,l)\ \ 0\le\theta<\frac{\pi}{2},\frac{3\pi}{2}\le\theta<2\pi\\ p''_{az}(\theta,l)=\sigma_{az1}(\theta,l)+\sigma_{az2}(\theta,l)+\sigma_{az4}(\theta,l)\ \ \frac{\pi}{2}\le\theta<\frac{3\pi}{2}\end{array}\right. \quad (15)$$



(**a**) Stage I (**b**) Stage II (**c**) Stage III

Figure 6. Schematic illustration for confining pressure redistribution of side tunnel under unloading of foundation pit.

The second stage is shown in Figure 6b. The additional load breaks the balance of the tunnel confining pressure, the longitudinal axis is deformed, and the entire cross section of the tunnel is displaced. Due to the uneven longitudinal deformation of the tunnel, relative displacement occurs between adjacent segment rings. The mutual restraint of the adjacent segment rings connected by the longitudinal bolts produces the between the segment rings so that the resultant force between the segment rings in the horizontal direction is F_{sx}, and the resultant force between the segment rings in the vertical direction is F_{sz}.

The third stage is shown in Figure 6c. The additional load on the side of the shield tunnel near the foundation pit will eventually be transferred to the other side through the tunnel structure, and the unloading will also appear on the side of the tunnel away from the foundation pit. For the convenience of analysis, the unloading on the side of the tunnel away from the foundation pit caused by the overall movement of the tunnel cross section to the foundation pit is simplified to a uniform distribution. It is assumed that the amount of the unloading on the side of the tunnel away from the foundation pit is p''_{ax}. At this time,

the deformation of the tunnel is stable, and the additional load in all directions satisfies the following formula:

$$\int_{\pi}^{2\pi} p'_{\mathrm{ax}}(\theta,l)\frac{D}{2}\mathrm{d}\theta = \int_{0}^{\pi} p''_{\mathrm{ax}}(\theta,l)\frac{D}{2}\mathrm{d}\theta + F_{\mathrm{sx}}(l) = p''_{\mathrm{ax}}(l)D + F_{\mathrm{sx}}(l) \tag{16}$$

$$\int_{0}^{\pi/2} p'_{\mathrm{az}}(\theta,l)\frac{D}{2}\mathrm{d}\theta + \int_{3\pi/2}^{2\pi} p'_{\mathrm{az}}(\theta,l)\frac{D}{2}\mathrm{d}\theta = \int_{\pi/2}^{3\pi/2} p''_{\mathrm{az}}(\theta,l)\frac{D}{2}\mathrm{d}\theta + F_{\mathrm{sz}}(l) \tag{17}$$

The vertical displacement of the shield tunnel beside the foundation pit is mainly caused by the asymmetric additional load in the vertical direction of the confining pressure. The uneven vertical displacement between the adjacent segment rings results in the vertical force between the segment rings. According to the vertical force balance as Equation (17), the resultant force between the segment rings in the vertical direction can be obtained by the following Equation:

$$F_{\mathrm{sz}}(l) = \int_{0}^{\pi/2} p'_{\mathrm{az}}(\theta,l)\frac{D}{2}\mathrm{d}\theta + \int_{3\pi/2}^{2\pi} p'_{\mathrm{az}}(\theta,l)\frac{D}{2}\mathrm{d}\theta - \int_{\pi/2}^{3\pi/2} p''_{\mathrm{az}}(\theta,l)\frac{D}{2}\mathrm{d}\theta \tag{18}$$

One of the key issues to consider the interaction of longitudinal deformation and transverse force is that how to consider the resultant force between the segment rings caused by longitudinal deformation of the tunnel when calculating the variation in confining pressure of the shield tunnel by the side of the foundation pit. According to the horizontal force balance as Equation (16), the amount of unloading on the side of the shield tunnel away from the foundation pit can be obtained as

$$p''_{\mathrm{ax}}(l) = \int_{\pi}^{2\pi} \frac{p'_{\mathrm{ax}}(\theta,l)}{2}\mathrm{d}\theta - \frac{F_{\mathrm{sx}}(l)}{D} \tag{19}$$

where $F_{\mathrm{sx}}(l)$ is the resultant force between the segment rings of the shield tunnel in the horizontal direction at the calculated section. The resultant force originates from the relative horizontal displacement between adjacent segment rings, that is, the deformation of the dislocation.

The authors of [20] have considered the collaborative effect of the rotation and dislocation deformation between the segment rings in the study of the longitudinal deformation of the shield tunnel, which can better reflect the characteristics of the longitudinal deformation of the shield tunnel structure. Therefore, the resultant force between the segment rings in the calculation process in this paper can be obtained by that method.

If the segment ring analyzed is located at $y = l$, then the horizontal displacement of the tunnel axis at this position is $u(l)$, and the horizontal shear force between the segment ring and adjacent segments of the former and latter rings can be expressed as $Q_{\mathrm{xF}}(l)$ and $Q_{\mathrm{xL}}(l)$, respectively. From the literature [20], we can obtain

$$Q_{\mathrm{xF}}(l) = j_{\mathrm{x}}[u(l - D_{\mathrm{t}}) - u(l)] \times k_{\mathrm{sl}} \tag{20}$$

$$Q_{\mathrm{xL}}(l) = j_{\mathrm{x}}[u(l) - u(l + D_{\mathrm{t}})] \times k_{\mathrm{sl}} \tag{21}$$

where j_{x} is the proportionality coefficient for the dislocation effects of the segment rings with the horizontal displacement of the tunnel axis, i.e., the ratio of the relative horizontal displacement generated by the dislocation between adjacent segment rings to the total relative horizontal displacement; D_{t} is the width of each segment ring; k_{sl} is the shear stiffness between segment rings of the shield tunnel.

The resultant force between the segment rings in the horizontal direction $F_{\mathrm{sx}}(l)$ on the segment ring at $y = l$ is

$$F_{\mathrm{sx}}(l) = Q_{\mathrm{xF}}(l) - Q_{\mathrm{xL}}(l) \tag{22}$$

Substituting the obtained $F_{sx}(l)$ into Equation (19) can obtain the amount of unloading on the side of the shield tunnel away from the foundation pit during the longitudinal deformation of the tunnel beside the foundation pit.

Comprehensive above, according to the distribution and variation of the additional load in all directions, the ultimate stable additional confining pressure of shield tunnel beside the foundation pit can be calculated as follows:

$$p_{ar}(\theta, l) = \begin{cases} p'_{az}(\theta, l)\cos\theta + p''_{ax}(l)\sin\theta, \ 0 \le \theta < \frac{\pi}{2} \\ p''_{az}(\theta, l)\cos\theta + p''_{ax}(l)\sin\theta, \ \frac{\pi}{2} \le \theta < \pi \\ p''_{az}(\theta, l)\cos\theta + p'_{ax}(\theta, l)\sin\theta, \ \pi \le \theta < \frac{3\pi}{2} \\ p'_{az}(\theta, l)\cos\theta + p'_{ax}(\theta, l)\sin\theta, \ \frac{3\pi}{2} \le \theta < 2\pi \end{cases} \tag{23}$$

4. Load Combination and Finite Element Model

4.1. Load Combination

Before the excavation of the foundation pit, the confining pressure of the side shield tunnel is composed of the initial load as shown in Figure 7, including (1) hydrostatic pressure p_w; (2) lateral active earth pressure p_e; (3) vertical earth pressure of overlying soil q; (4) structure weight g; (5) arch bottom reaction force q_R; (6) lateral soil resistance p_k. According to the method in Section 3.3 of this paper, the additional load distribution after the deformation of the tunnel beside the foundation pit is stabilized can be calculated, as shown in Figure 6c.

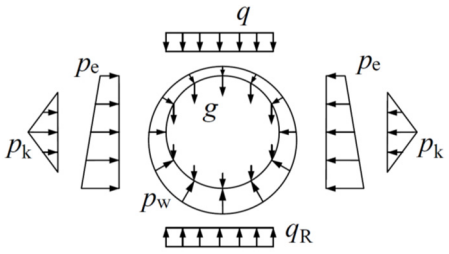


Figure 7. Schematic illustration for initial load combination.

4.2. Finite Element Model

In this research, finite element software MIDAS is used to establish a simplified segment ring model of shield tunnel. As shown in Figure 8, to simplify the calculation, this paper uses a two-dimensional finite element model for structural calculations. The segment ring is composed of a seal roof block, two adjacent blocks, and three standard blocks, and the segment blocks are simplified as a beam element for simulation. Referring to the beam–joint model in the literature [32], it uses two-node elastic connection elements to simulate segment joints in this paper, to make the simplified model more consistent with the actual mechanical behavior of segment rings. As shown in Figure 8, the joint element is composed of two nodes, and the relationship between internal force and deformation is

$$\begin{Bmatrix} N_2 - N_1 \\ Q_2 - Q_1 \\ M_2 - M_1 \end{Bmatrix} = \begin{bmatrix} k_n & & \\ & k_s & \\ & & k_\theta \end{bmatrix} \begin{Bmatrix} \Delta u \\ \Delta v \\ \Delta\theta \end{Bmatrix} \tag{24}$$

where N_1, Q_1, M_1 and N_2, Q_2, M_2 are the forces acting on nodes 1 and 2 in various directions, as shown in Figure 8; k_n, k_s, and k_θ are the axial, tangential and rotational stiffness of the joint unit, respectively, the value can be found in the literature [33]; Δu, Δv, and $\Delta\theta$ are the axial deformation, tangential deformation, and relative rotation angle of the joint unit in the local coordinate system, respectively.

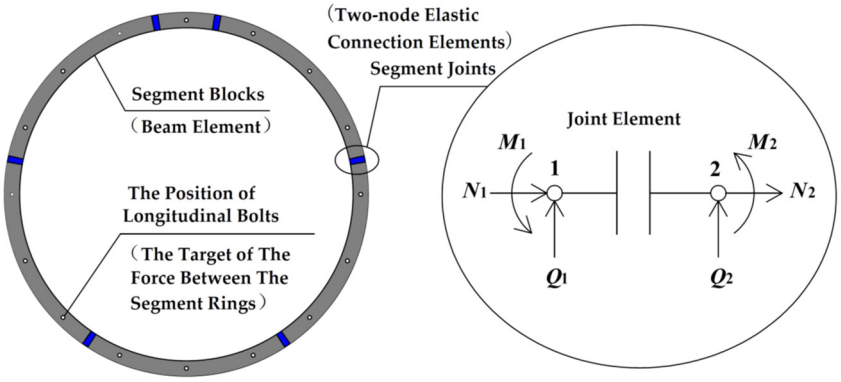


Figure 8. Schematic diagram of finite element model of shield tunnel segment and joint element.

The structural analysis process is divided into two stages, to apply the loads. In the first stage, the initial confining pressure is applied to the segment structure according to the initial load combination in Section 4.1. At this stage, the internal force of the tunnel's segment ring under the initial working condition can be calculated. In the second stage, on the basis of the first stage, the additional confining pressure after the deformation of the tunnel is stabilized and applied to the segment unit, and the resultant force between the segment rings of the calculated section segment and the adjacent segment is applied to the position of each longitudinal bolt. Then, calculation and analysis are performed to obtain the internal force of the existing shield tunnel caused by the excavation of the foundation pit.

5. Analysis of Engineering Case

5.1. Project Profile

Take the deep foundation pit project by the side of the shield tunnel of Hangzhou Metro Line 2 as a case study, which has been put into operation at the intersection of Shixinzhong Road and Jincheng Road in Xiaoshan District. The plane size of the foundation pit excavation is L = 68 m, B = 72 m, with the excavation depth H_e = 15.8 m, and the underground diaphragm wall is 37.2 m below the ground. According to the field measured data in this engineering case, the deformation control parameter of the retaining structure is approximately v_{max}/H_e = 0.2% (i.e., the accumulated maximum deformation after the excavation is 0.2% of the excavation depth). Minimum clearance from the sideline of the foundation pit's retaining structure to the tunnel is s = 9.5 m [34]. The tunnel is buried 14.3 m deep in the silty silt and sandy silt layer. The outer diameter of the shield tunnel is D = 6.2 m, which adopted C50 concrete segments, the thickness of the segment is t = 0.35 m, the ring width is D_t = 1.2 m. The elastic modulus of the segment is 34.5 GPa, and the Poisson's ratio is 0.2. The segment ring is composed of six concrete segments, including one seal roof block with a central angle of 20°, two adjacent blocks with a central angle of 68.75°, and three standard blocks with a central angle of 67.5°. The parameter values of the segment joint unit are $k_n = 7.09 \times 10^8$ kN/m, $k_s = 1.86 \times 10^5$ kN/m and $k_\theta = 4 \times 10^5$ kN·m/rad. A total of 16 M30 longitudinal bolts were used to connect the adjacent segment rings, and the shear stiffness between segment rings is $k_{sl} = 2.23 \times 10^6$ kN/m. The water level near the tunnel fluctuates slightly, about 1.02 m below the ground. Table 1 shows the distribution and parameters of the soil layer within the scope of foundation pit excavation.

Table 1. Soil layer parameters and distribution.

Number	Soil Layer	Thickness (m)	Saturation Weight γ_{sat} (kN/m^3)	Cohesion c (kPa)	Interior Friction Angle φ (°)
2–1	Silty clay	1.7	19.3	25.6	10.0
3–1	Sandy silt	4.0	18.6	3.1	25.5
3–2	Sandy silt	2.8	19.4	3.2	25.8
3–3	Mixture of sandy silt and silt	4.3	19.9	3.7	26.0
3–4	Sandy silt	2.0	19.2	3.5	25.6
4–1	Mucky silty clay	13.3	17.4	19.8	8.2

5.2. Calculation and Analysis Results

Using the method in this paper, the confining pressure of the shield tunnel before and after the excavation of the foundation pit is calculated, and the section at l = 0 m is taken as an example, as shown in Figure 9. Before the excavation of the foundation pit, as the water and soil pressures increase with the increase in depth, the calculated confining pressure of the shield tunnel is small in the upper part and larger in the lower part, and is symmetrically distributed in a "bell shape." Taking the ring's upper vertex as 0°, the angle increases clockwise. The maximum confining pressure is 244.96 kPa, which is located near 150°. After the excavation of the foundation pit, the confining pressure on both sides of the tunnel decreased significantly, and the confining pressure at the top increased slightly.

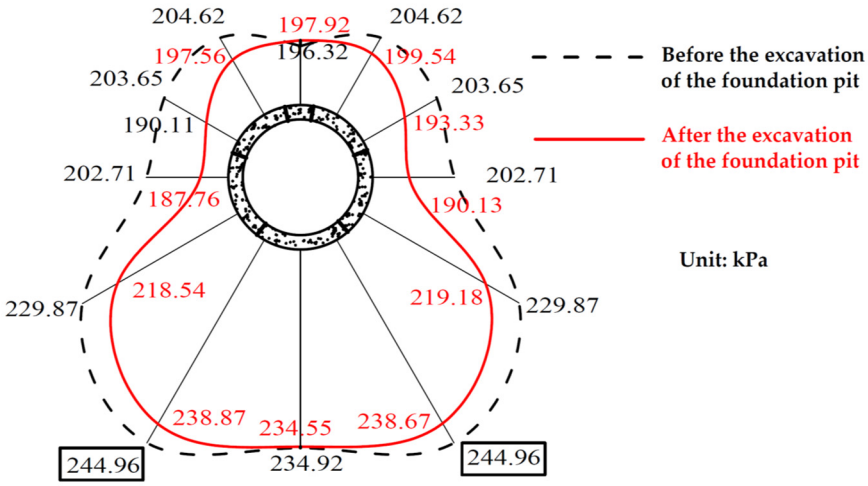


Figure 9. Variation diagram for confining pressure of side shield tunnel caused by excavation of foundation pit.

Figure 10 shows the additional confining pressure distribution of the tunnel by the side of the foundation pit calculated by the method in this paper and the literature [19]. It can be seen from the figure, the results of the method in this paper show that the additional confining pressure in most areas is negative except for a small positive value at the top of the tunnel, that is, the excavation of the foundation pit mainly causes the decrease in the confining pressure on the side tunnel. In this case, the unloading effect of the tunnel at 285° is the most obvious, and the value of the additional confining pressure is −15 kPa, which is 7.34% less than the confining pressure before the excavation of the foundation pit.

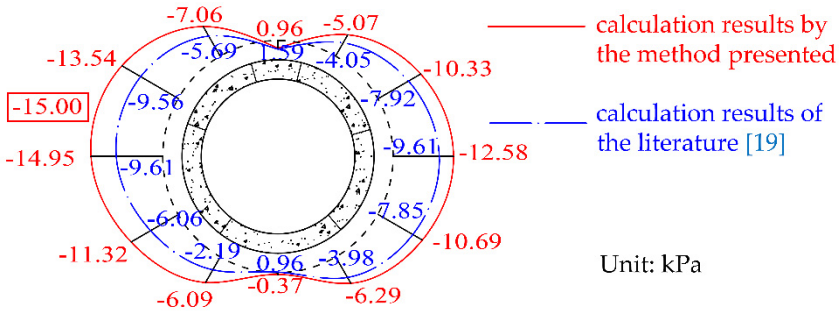
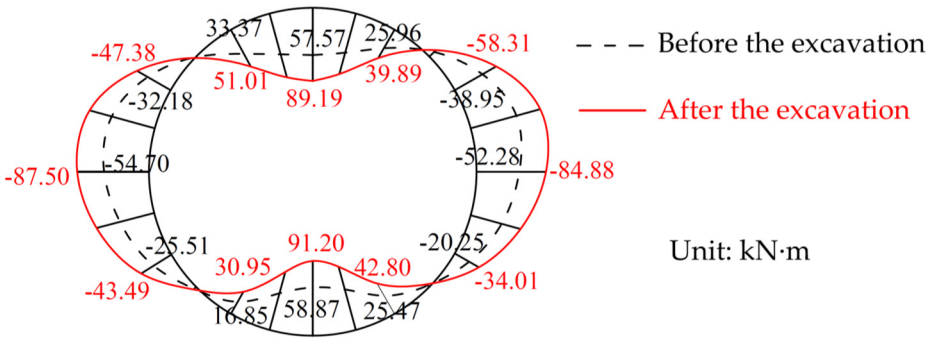


Figure 10. Additional confining pressure distribution of shield tunnel by the side of foundation pit.

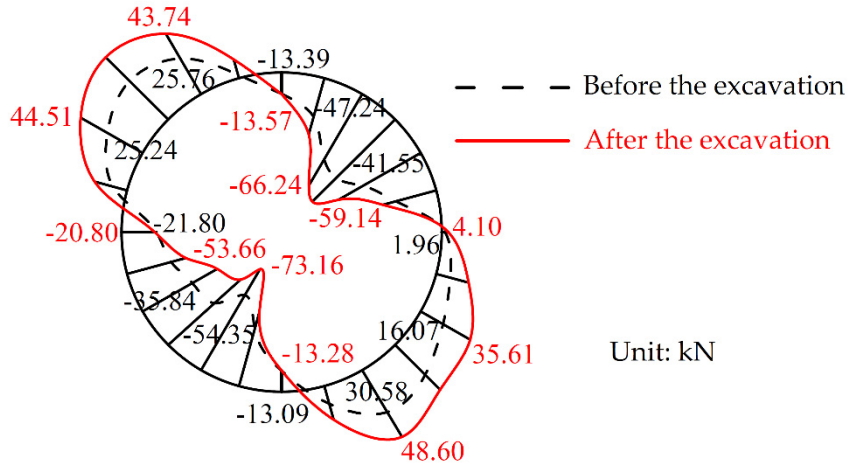
As shown in Figure 10, except for the positions of 0° and 180°, the absolute value of the additional confining pressure calculated by the method presented in this paper is greater than the calculation results of the literature [19], especially the unloading amount of the confining pressure on the left side (the side near the foundation pit) has a significant difference, compared with the literature [19]; the maximum unloading amount obtained by the method in this paper has increased by 56.3%, and the calculation results of the method in this paper show more obvious asymmetry. The model test results in the literature [35] show that the confining pressure reduction of the closest point of the tunnel beside the foundation pit will be significantly greater than the farthest point; therefore, the results obtained by the method presented in this paper are more consistent with the law presented by the model test data.

Figure 11a–c is the calculation results of the internal force of the tunnel's segment ring before and after the excavation obtained by the finite element model. Table 2 shows the comparison of the extreme internal force and its position distribution before and after the excavation of the foundation pit. As shown in Figure 11a, the segment ring's top and bottom present a positive bending moment, which is tensioned on the inside, and a negative bending moment at the arch waist, which is tensioned on the outside. It can be obtained from Table 2 that before the excavation of the foundation pit, the maximum positive bending moment is 58.87 kN·m, which is located at 180°, and the maximum negative bending moment is −58.03 kN·m, which is located at 75°. After the excavation of the foundation pit, the absolute value of the positive and negative bending moments both increased, of which the maximum positive bending moment was 91.20 kN·m, an increase of 54.90%, compared to the initial conditions. The maximum negative bending moment is −88.14kN·m, and the absolute value is 51.88% higher than that before excavation.

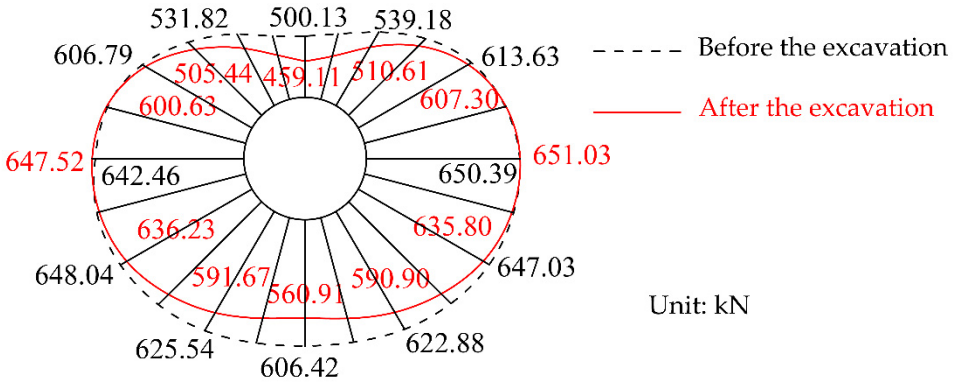


(**a**) Bending moment diagram

Figure 11. *Cont.*



(**b**) Shear force diagram



(**c**) Axial force diagram

Figure 11. Variation diagram for internal force of shield tunnel by the side of foundation pit.

Table 2. Statistical comparison of extreme value and distribution position of internal force in tunnel.

Internal Force		Before the Excavation		After the Excavation	
		Extreme Value	Position	Extreme Value	Position
Bending Moment	Maximum	58.87 kN·m	180°	91.20 kN·m	180°
	Minimum	−58.03 kN·m	75°	−88.14 kN·m	75°
Shear Force	Maximum	34.00 kN	315°	55.12 kN	315°
	Minimum	−54.35 kN	210°	−73.16 kN	210°
Axial Force	Maximum	651.74 kN	105°	651.03 kN	90°
	Minimum	500.13 kN	0°	459.11 kN	0°

As shown in Figure 11b, the shape of the shear force diagram of the tunnel is irregular due to the existing joints in the segment ring. As shown in Table 2, before the excavation of the foundation pit, the maximum positive and negative shear values are located at 315° and 210°, respectively, which are 34 kN and −54.35 kN. After the excavation of the foundation pit, the maximum positive shear value increased to 55.12 kN, and the absolute value of the maximum negative shear force increased to 73.16 kN, an increase of 62.15% and 34.60%, respectively, from the initial conditions.

As shown in Figure 11c, the maximum axial force of the segment ring is located at the waist, while the top axial force is the smallest. It can be seen from Table 2 that the excavation of the foundation pit mainly causes the decrease in the axial force at the top and bottom of the shield tunnel. The axial forces at 0° and 180° at the initial working conditions are 500.13 kN and 606.42 kN, respectively. The excavation of the pit reduced it to 459.11 kN and 560.91 kN, respectively, a decrease of 8.20% and 7.50%.

6. Analyze the Influence Factors of Adjacent Tunnel's Transverse Force

6.1. Deformation the Foundation Pit Retaining Structure

In engineering applications, the accumulated maximum deformation of the foundation pit retaining structure is usually taken as the deformation control index of the retaining structure. Statistics of measured data show that the cumulative maximum deformation (v_{max}) of the retaining structure is closely related to the excavation depth (H_e), Therefore, the deformation control parameter (v_{max}/H_e) can reflect the deformation control situation for the foundation pit. Taking the engineering case in this paper as the basic working condition, we changed the deformation control parameter (v_{max}/H_e) of the foundation pit retaining structure under the condition that other parameters remain constant.

Figure 12 shows the additional confining pressure of the shield tunnel by the side of the foundation pit obtained by the method presented in this paper when the deformation control parameter v_{max}/H_e of the foundation pit retaining structure is controlled at 0.05%, 0.10%, 0.15% and 0.20%, respectively. It can be seen from the figure that most of the additional confining pressures of the tunnel by the side of the foundation pit are negative, that is, the confining pressure decreases, and the maximum absolute value of the additional confining pressure appears in the range of 270~285° on the side near the foundation pit (the left side). With the increase in the deformation control parameter v_{max}/H_e of the retaining structure of the foundation pit, the unloading amount of the tunnel confining pressure increases. When v_{max}/H_e is, respectively, taken as 0.05%, 0.10%, 0.15% and 0.20%, the maximum absolute values of the additional confining pressure are 4.76 kPa, 9.09 kPa, 12.60 kPa and 15.00 kPa, respectively, which are the 2.35%, 4.48%, 6.16% and 7.34% of initial confining pressures at the corresponding positions before the excavation of the foundation pit.

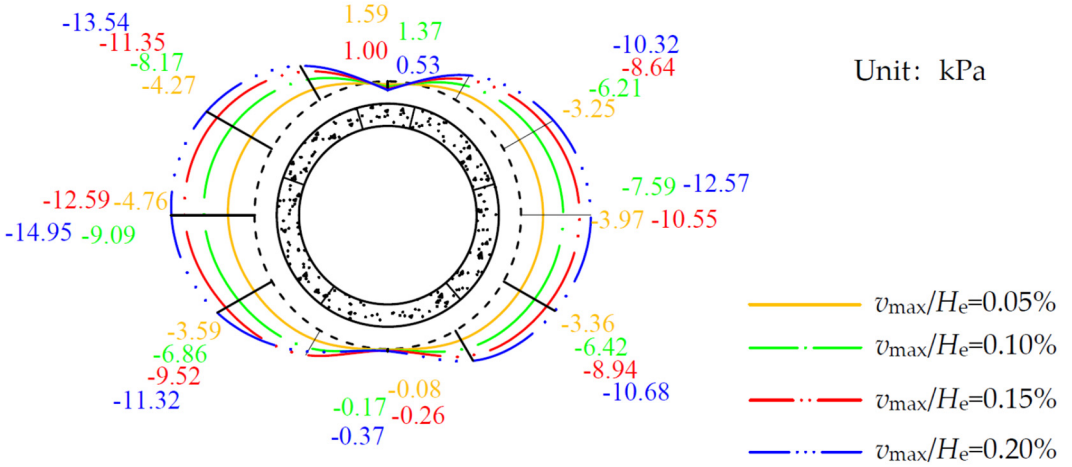


Figure 12. Distribution of additional confining pressure of adjacent shield tunnel at different v_{max}/H_e.

Figure 13 is a comparison diagram of the additional bending moment of the adjacent shield tunnel caused by the foundation pit excavation when the deformation control parameter v_{max}/H_e of the foundation pit retaining structure takes different values. As shown in the figure, the positive and negative additional bending moments on the tunnel both increase with the increase in v_{max}/H_e. Additionally, the maximum additional positive bending moments are all located at the bottom, and the maximum additional negative

bending moments are all located at the waist that closes to the foundation pit (the left side). When v_{max}/H_e = 0.05%, the positive bending moment at the bottom of the tunnel's segment ring increases by 10.31 kN·m, and the absolute value of the negative bending moment at the waist that closes to the foundation pit (the left side) increases by 10.48 kN·m, which are, respectively, 17.51% and 19.15% of the absolute value of the initial bending moment at the corresponding position before the excavation of the foundation pit. When v_{max}/H_e increased to 0.20%, the positive bending moment at the bottom of the tunnel's segment ring increases by 32.32 kN·m, and the absolute value of the negative bending moment at the waist that closes to the foundation pit (the left side) increases by 32.80 kN·m, which are, respectively, 54.89% and 59.96% of the absolute value of the initial bending moment at the corresponding position before the excavation of the foundation pit. According to Figures 12 and 13, it can be found that the response of the tunnel's segment ring bending moment to the excavation unloading of the foundation pit is more obvious than the variation of confining pressure value.

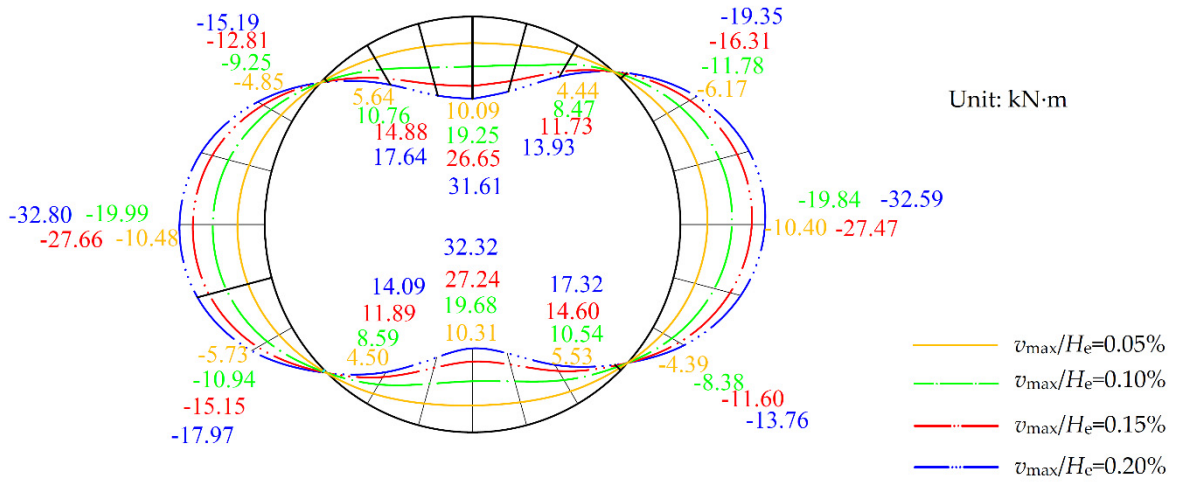


Figure 13. Comparison diagram of the additional bending moment when the deformation control parameter v_{max}/H_e of the foundation pit retaining structure takes different values.

6.2. The Clearance between Foundation Pit and Tunnel

Taking the engineering case in this paper as the basic working condition, under the condition that other parameters remain constant, we only changed the clearance s between the foundation pit and the adjacent tunnel. Figure 14 shows the additional confining pressure distribution of the shield tunnel by the side of the foundation pit obtained by the method presented in this paper when s is taken as 4/3 H_e, H_e, 2/3 H_e and 1/3 H_e, respectively. It can be seen from the figure that as the clearance between the foundation pit and the adjacent tunnel decreases, the absolute value of the additional confining pressure of the tunnel caused by the excavation of the foundation pit increases. When the clearance between the foundation pit and the adjacent tunnel is reduced from 4/3 H_e to 2/3 H_e, the absolute value of the additional confining pressure on the tunnel increases slightly. When the clearance between the foundation pit and the adjacent tunnel is further reduced to 1/3 H_e, the absolute value of the additional confining pressure in the range of 270~360° (the side closes to the foundation pit) increases significantly. At this time, the maximum absolute value of the additional confining pressure is 20.87 kPa, which is 10.21% of the initial confining pressure at the corresponding position.

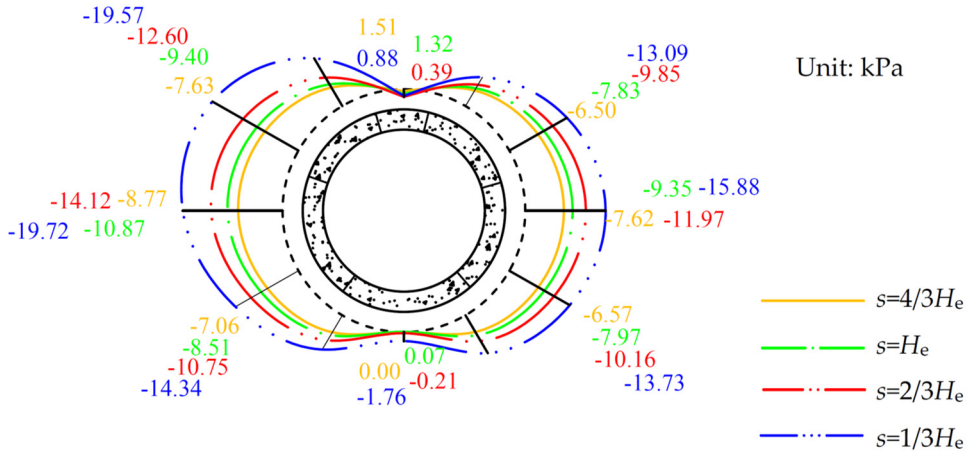


Figure 14. Distribution of additional confining pressure of tunnel with different clearance *s* between tunnel and pit.

Figure 15 is a comparison diagram of the additional bending moment of the adjacent shield tunnel caused by the foundation pit excavation when the clearance *s* between the foundation pit and the adjacent tunnel takes different values. As shown in the figure, as the clearance *s* between the foundation pit and the adjacent tunnel decreases, the additional positive and negative bending moments of the shield tunnel's segment ring both increase. The clearance *s* is reduced from 4/3 H_e to 1/3 H_e, the maximum additional positive bending moment at the bottom of the segment ring is increased from 19.04 kN·m to 39.20 kN·m, and the absolute value of the maximum additional negative bending moment at the waist that closes to the foundation pit (the left side) increases from 19.24 kN·m to 39.47 kN·m.

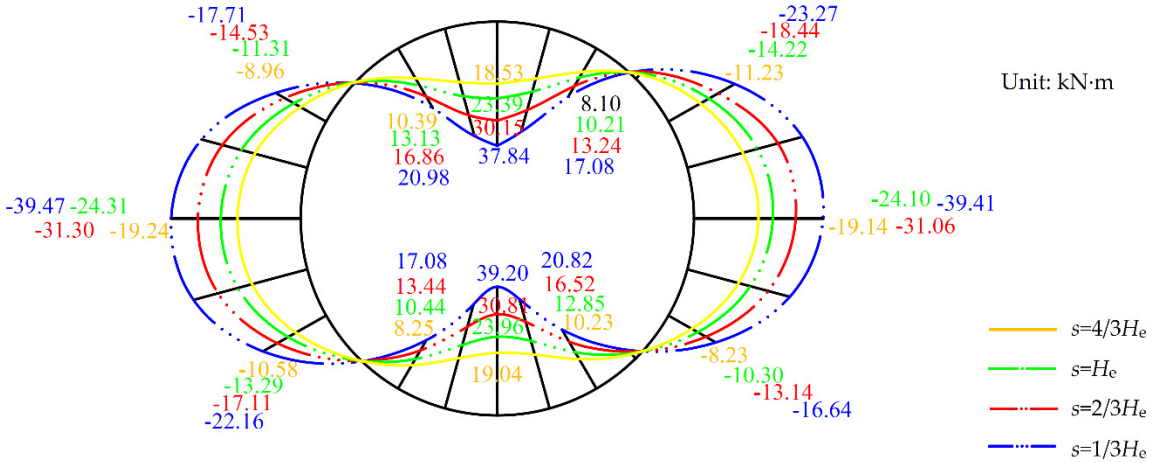


Figure 15. Comparison diagram of the additional bending moment when the clearance *s* between the foundation pit and the adjacent tunnel takes different values.

6.3. The Buried Depth of Tunnel

Taking the engineering case in this paper as the basic working condition, under the condition that other parameters remain constant, we only changed the buried depth *h* of the axis of the tunnel by the side of the foundation pit. Figure 16 shows the additional confining pressure distribution of the shield tunnel by the side of the foundation pit obtained by the method presented in this paper when *h* is taken as 2/3 H_e, H_e, 4/3 H_e and 5/3 H_e, respectively. When the buried depth of the axis of the tunnel by the side of the foundation pit is h = 2/3 H_e, the maximum absolute value of the additional confining pressure is 16.94 kPa, which means that the confining pressure is 12.39% lower than that before the excavation of the foundation pit. As the buried depth *h* increases, the impact on the

tunnel caused by the foundation pit excavation will decrease. When the buried depth h exceeds the excavation depth H_e of the foundation pit, the absolute value of the additional confining pressure will be reduced significantly. When the buried depth of axis of the tunnel by the side of the foundation pit increase to $h = 5/3\ H_e$, the additional confining pressure is more evenly distributed on the tunnel, and the maximum absolute value of the additional confining pressure is the only 4.31 kPa, which is located on the position of 315°, the confining pressure is only reduced by 1.02% compared with that before the excavation of the foundation pit.

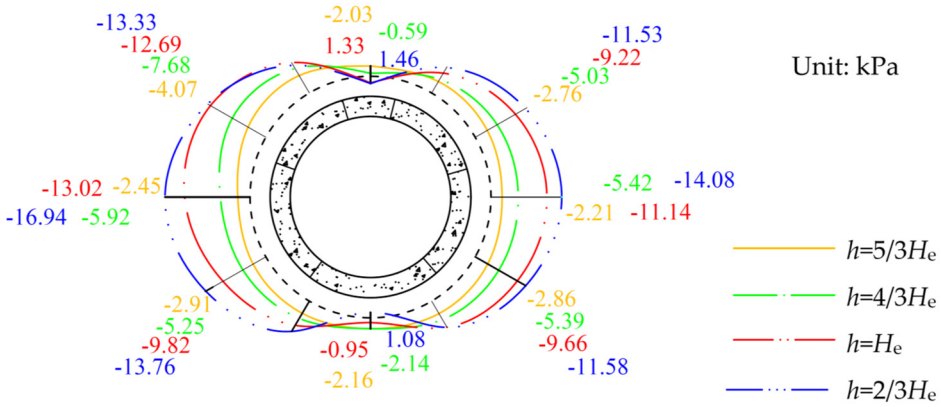


Figure 16. Distribution of additional confining pressure of adjacent tunnel with different buried depth *h*.

Figure 17 is a comparison diagram of the additional bending moment of the adjacent shield tunnel's segment ring caused by the foundation pit excavation when the buried depth h takes different values. As shown in the figure, as the buried depth h increases, the positive and negative additional bending moments caused by the foundation pit excavation will decrease accordingly. When the buried depth h of the tunnel exceeds the excavation depth H_e of the foundation pit, the positive and negative additional bending moments are significantly reduced. When the buried depth of the tunnel continues to increase to $h = 5/3\ H_e$, the positive and negative additional bending moments of the tunnel's segment ring are already very small, and their absolute values are both less than 1 kN·m. According to the analysis of Figures 16 and 17, the foundation pit excavation has a greater impact on the adjacent shield tunnel with a shallow buried depth. When the buried depth exceeds the excavation depth of the foundation pit, the influence of the foundation pit excavation is significantly weakened.

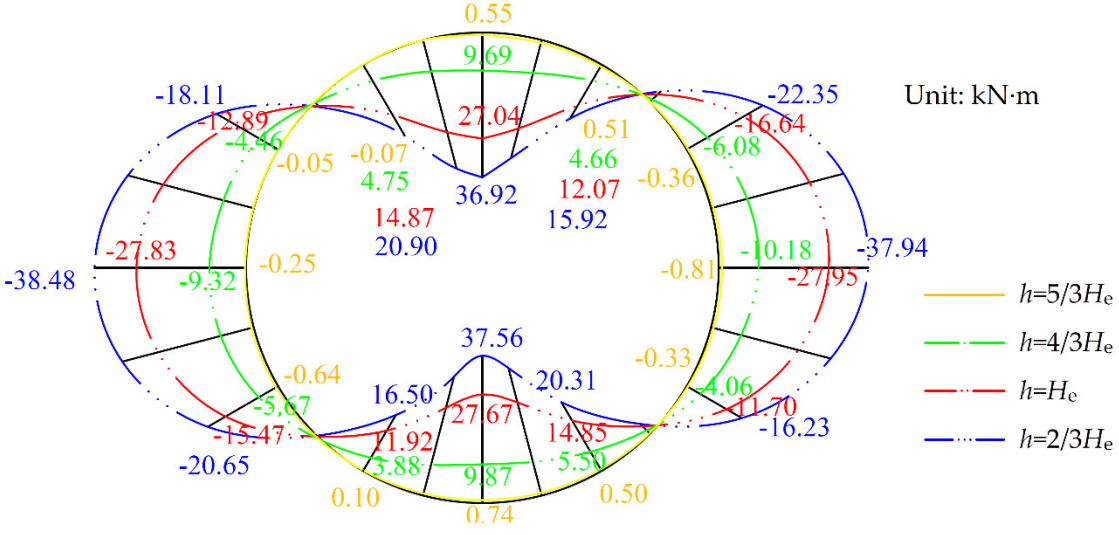


Figure 17. Comparison diagram of the additional bending moment when the buried depth *h* takes different values.

7. Conclusions and Further Research

In this paper, a variation in the transverse additional confining pressure model for the shield tunnel considering the effect of longitudinal deformation was established. The effect of the unloading of the foundation pit's sidewall on the adjacent shield tunnel was analyzed with an unloading model of the sidewall, which considers both the foundation pit's deformation of retaining structure and the spatial effect. Meanwhile, the calculation case based on the actual engineering and the analysis of influence factors was carried out. Thus, the following conclusions are drawn:

(1) The foundation pit excavation causes a decrease in the confining pressure of the adjacent shield tunnel, especially, the confining pressure on the tunnel's waist, which is near the side of the foundation pit. Compared with the existing theoretical methods, the calculation results of the additional confining pressure of the method presented in this paper can better reflect the asymmetry of the confining pressure of the tunnel by the side of the foundation pit.

(2) The positive and negative bending moment and the positive and negative shear force on the adjacent shield tunnel's segment ring both increase due to the foundation pit excavation, and it also causes the decrease in the axial force on the top and bottom of the adjacent shield tunnel's segment ring. With the increase in the deformation control parameter $v_{\max}/H_e$ of the foundation pit's retaining structure, the absolute value of the additional confining pressure of the adjacent tunnel increases. The response of the tunnel's segment ring bending moment to the excavation unloading of the foundation pit is more obvious than the variation of confining pressure value.

(3) The foundation pit excavation has more impact on the adjacent shield tunnels with shallow buried depth. When the buried depth of the tunnel is deeper than the excavation depth of the foundation pit, the influence of the foundation pit excavation will be significantly weakened. As the clearance between the pit and tunnel decreases, the influence of the foundation pit excavation on the adjacent shield tunnel will be enhanced.

The method and analysis results presented in this paper have guiding significance for the experimental research of this engineering problem and design for the foundation pit near the shield tunnel. However, due to the fact that the measured data of transverse force of tunnel are rare and difficult to obtain, the reliability of the analysis results needs further verification. Therefore, it is suggested to carry out more experimental research on this problem. Furthermore, only one deformation mode of the foundation pit retaining structure is considered in this study, and the tunnel structure analysis adopts a simplified two-dimensional finite element structure model. After that, it is necessary to study the different deformation modes of foundation pits, and further refine the analysis of the segment structure.

Author Contributions: Conceptualization, methodology, software and original draft preparation, X.Z.; conceptualization, guidance, review and revision, G.W.; original draft preparation, translation, editing and review, X.L. review and revision, C.X.; guidance, review and revision, X.W. All authors have read and agreed to the published version of the manuscript.

Funding: This research was supported by The General Scientific Research Projects for Agriculture and Social Development in Hangzhou (20201203B127) and The National Natural Science Foundation of China (Grant No. 51778576).

Acknowledgments: We are grateful to other members of our research team (Wang, X.; Qi, Y.J.; Zhou, X.X.; Feng, F.F.) for their support.

Conflicts of Interest: The authors declare no conflict of interest.

References

1. Yan, J.Y.; Wang, R.L. Cause analysis and typical characteristics of settlement and transverse convergence deformation of metro tunnel in soft ground in Shanghai. *J. Nat. Disasters* **2018**, *27*, 178–187. (In Chinese)
2. Wang, H. Influence of deep excavation on the adjacent existing shielded subway tunnels. *Soil Eng. Found.* **2019**, *33*, 19–22. (In Chinese)
3. Yang, Y.B.; Zhou, B.; Xie, X.Y. Study on transverse deformation and cracking property of shield-driven tunnel induced by adjacent excavation. *Chin. J. Rock Mech. Eng.* **2016**, *35*, 4082–4093. (In Chinese)
4. Zhou, Z.L.; Chen, S.G.; Tu, P.; Zhang, H.S. An analytic study on the deflection of subway tunnel due to adjacent excavation of foundation pit. *J. Mod. Transp.* **2015**, *23*, 287–297. [CrossRef]
5. Zhang, Z.G.; Zhang, M.X.; Wang, W.D. Two-stage method for analyzing effects on adjacent metro tunnels due to foundation pit excavation. *Rock Soil Mech.* **2011**, *32*, 2085–2092. (In Chinese)
6. Liang, R.Z.; Xia, T.D.; Huang, M.S.; Lin, C.G. Simplified method for evaluating the effects of adjacent excavation on shield tunnel considering the shearing effect. *Comput. Geotech.* **2017**, *81*, 167–187. [CrossRef]
7. Liang, R.Z.; Wu, W.B.; Yu, F.; Jiang, G.S.; Liu, J.W. Simplified method for evaluating shield tunnel deformation due to adjacent excavation. *Tunn. Undergr. Space Technol.* **2018**, *71*, 94–105. [CrossRef]
8. Zhang, Z.G.; Huang, M.S.; Wang, W.D. Evaluation of deformation response for adjacent tunnels due to soil unloading in excavation engineering. *Tunn. Undergr. Space Technol.* **2013**, *38*, 244–253. [CrossRef]
9. Zhang, J.F.; Chen, J.J.; Wang, J.H.; Zhu, Y.F. Prediction of tunnel displacement induced by adjacent excavation in soft soil. *Tunn. Undergr. Space Technol.* **2013**, *36*, 24–33. [CrossRef]
10. Zheng, G.; Du, Y.M.; Cheng, X.S.; Diao, Y.; Deng, X.; Wang, F.J. Characteristics and prediction methods for tunnel deformations induced by excavations. *Geomech. Eng.* **2017**, *12*, 361–397. [CrossRef]
11. Shi, J.W.; Ng, C.W.W.; Chen, Y.H. Three-dimensional numerical parametric study of the influence of basement excavation on existing tunnel. *Comput. Geotech.* **2015**, *63*, 146–158. [CrossRef]
12. Chen, R.; Meng, F.; Li, Z.; Ye, Y.; Ye, J. Investigation of response of metro tunnels due to adjacent large excavation and protective measures in soft soils. *Tunn. Undergr. Space Technol.* **2016**, *58*, 224–235. [CrossRef]
13. Devriendt, M.; Doughty, L.; Morrison, P.; Pillai, A. Displacement of tunnels from a basement excavation in London. *Geomech. Eng.* **2010**, *163*, 131–145. [CrossRef]
14. Ng, C.W.W.; Shi, J.W.; Mašín, D.; Sun, H.S.; Lei, G.H. Influence of sand density and retaining wall stiffness on the three-dimensional responses of a tunnel to basement excavation. *Can. Geotech. J.* **2015**, *52*, 1811–1829. [CrossRef]
15. Wang, L.F.; Pang, J.; Xu, Y.F.; Yang, K.F. Influence of foundation pit excavation on adjacent metro tunnels. *Rock Soil Mech.* **2016**, *37*, 2004–2010. (In Chinese)
16. Simpson, B.; Vardanega, P.J. Results of monitoring at the British Library excavation. *Proc. Inst. Civ. Eng. Geotech. Eng.* **2014**, *167*, 99–116. [CrossRef]
17. Hu, H.Y.; Zhang, Y.C.; Yang, G.H.; Zhong, Z.H.; Chen, F.Q. Measurement and numerical analysis of effect of excavation of foundation pits on metro tunnels. *Chin. J. Geotech. Eng.* **2014**, *36*, 431–439. (In Chinese)
18. Chen, R.P.; Ashraf, A.M.; Meng, F.Y. Three-dimensional centrifuge modeling of influence of nearby excavations on existing tunnels and effects of cut-offwalls. *Chin. J. Geotech. Eng.* **2018**, *40*, 6–11. (In Chinese)
19. Wei, G.; Zhang, X.H.; Lin, X.B. Variations of transverse forces on nearby shield tunnel caused by foundation pits excavation. *Rock Soil Mech.* **2020**, *41*, 635–644. (In Chinese)
20. Zhang, X.; Wei, G.; Jiang, C. The Study for Longitudinal Deformation of Adjacent Shield Tunnel Due to Foundation Pit Excavation with Consideration of the Retaining Structure Deformation. *Symmetry* **2020**, *12*, 2103. [CrossRef]
21. Zhou, S.H.; He, C.; Xiao, J.H. Energy method for calculating deformation of adjacent shield tunnels due to foundation pit excavation considering step between rings. *China Railw. Sci.* **2016**, *37*, 53–60. (In Chinese)
22. Jiang, Z.H.; Zhang, Y.X. Calculation of influence on longitudinal deformation of adjacent tunnels due to excavation. *J. Chongqing Jianzhu Univ.* **2013**, *35*, 7–11. (In Chinese)
23. Wei, G.; Zhao, C.L. Calculation method of additional load of adjacent metro tunnels due to foundation pit excavation. *Chin. J. Rock Mech. Eng.* **2016**, *35*, 3408–3417. (In Chinese)
24. Ding, Z.; Wang, D.; Wang, J.Y.; Wei, X.J. Deformation characteristics of Zhejiang soft soil deep foundation pits and their predictive analysis. *Rock Soil Mech.* **2015**, *36*, 506–512. (In Chinese)
25. Liu, M.L.; Fang, Q.; Zhang, D.L.; Hou, Y.J. Prediction of transient deformation due to excavation based on improved MSD method. *Chin. J. Rock Mech. Eng.* **2018**, *37*, 1700–1707. (In Chinese)
26. Ou, C.Y.; Chiou, D.C.; Wu, T.S. Three-Dimensional finite element analysis of deep excavations. *J. Geotech. Eng.* **1996**, *122*, 337–345. [CrossRef]
27. Liu, N.W.; Gong, X.N.; Yu, F.; Fang, K. Analysis of spatial effects in strutted excavation and related influential factors. *Rock Soil Mech.* **2014**, *35*, 2293–2298. (In Chinese)
28. Finno, R.J.; Blackburn, J.T.; Roboski, J.F. Three-Dimensional effects for supported excavations in clay. *Am. Soc. Civ. Eng.* **2007**, *133*, 30–36. [CrossRef]
29. Xu, R.Q. Methods of earth pressure calculation for excavation. *J. Zhejiang Univ. Eng. Sci.* **2000**, *34*, 370–375. (In Chinese)

30. Ke, C.T.; Chen, Y.B.; Gao, H.B.; Cao, X. Calculation model and application of non-limit earth pressure considering displacement of retaining structure. *Water Resour. Power* **2013**, *31*, 127–131. (In Chinese)
31. Mindlin, R.D. Force at a point in the interior of a semi-infinite solid. *Physics* **1936**, *7*, 195–201. [CrossRef]
32. Zhu, H.H.; Zhou, L.; Zhu, J.W. Beam-spring generalized model for segmental lining and simulation of its nonlinear rotation. *Chin. J. Geotech. Eng.* **2019**, *41*, 1581–1590. (In Chinese)
33. Yan, Q.X.; Chen, H.; Chen, W.Y. Analytical method and parameters study of ring joint stiffness of shield tunnel. *J. Cent. South Univ. Sci. Technol.* **2018**, *49*, 1555–1565. (In Chinese)
34. Wei, G.; Li, J.; Xuan, H.L.; Dong, L.Z.; Xu, Y.Y.; Zhang, S.M. Monitoring data analysis on the influence of large deep foundation pit excavation on nearby metro shield tunnel. *J. Railw. Sci. Eng.* **2018**, *15*, 718–726. (In Chinese)
35. Hu, X. Influence of foundation pit excavation under different conditions simulating by model test on existing tunnel. *Subgrade Eng.* **2015**, *6*, 151–155. (In Chinese)